Phys. Status Solidi B **250**, No. 7, 1293–1299 (2013) / **DOI** 10.1002/pssb.201248225

physica status solidi b
www.pss-b.com
basic solid state physics

Elastic anisotropy and thermodynamic properties of tetrahedrally bonded dense $C_2N_2(NH)$ under high pressure and high temperature

Haiyan Yan[*,1], **Meiguang Zhang**[2], **Qun Wei**[**,3], **and Ping Guo**[4]

[1] Department of Chemistry and Chemical Engineering, Baoji University of Arts and Sciences, Baoji 721013, P. R. China
[2] Department of Physics, Baoji University of Arts and Sciences, Baoji 721016, P. R. China
[3] School of Science, Xidian University, Xi'an 710071, P. R. China
[4] Department of Physics, Northwest University, Xi'an 710069, P. R. China

Received 22 May 2012, revised 20 August 2012, accepted 30 October 2012

Keywords carbon nitride, elastic anisotropy, first-principles calculations, thermodynamic properties

---

[*] Corresponding author: e-mail hyyan1102@163.com, Phone/Fax: 86 917 3566589
[**] Corresponding author: e-mail weiaqun@163.com, Phone/Fax: 86 29 88469165

The elastic anisotropy and thermodynamic properties of the potential superhard carbon nitride phase $C_2N_2(NH)$ have been investigated by using an *ab initio* plane-wave pseudopotential density theory method. The crystal parameters have been calculated at ambient as well as high pressure. The Young's modulus and shear modulus as a function of crystal orientations for $C_2N_2(NH)$ have been systematically investigated. The Young's modulus is found to reach a maximum along the [100] direction. Using a set of total energy versus volume obtained with the first-principles calculations, the quasiharmonic Debye model is applied to the study of the thermal and vibrational effects. The dependence of Debye temperature, Grüneisen parameter, heat capacity, and expansion coefficient on the temperature and pressure are systematically explored in the whole pressure range from 0 to 60 GPa and temperature range from 0 to 2000 K.

1 Introduction

Superhard materials are important in modern high-pressure science and technology due to their outstanding properties, such as ultraincompressible, high elastic modulus, high hardness, and scratch resistance [1]. It is generally accepted that the superhard materials are those strong covalent compounds formed by light elements B, C, N, and O. The intrinsically strong and directional covalent bonds between these light elements lead to tight, three-dimensional crystalline networks with extreme resistance to external shear. In the past two decades, the binary C–N system has been studied extensively as potential candidate for extraordinary hardness materials. It has been theoretically predicted that sp^3-bonded forms of carbon nitride (β-C_3N_4) can be superhard [2, 3]. Since then, there have been intense interests in developing high-density materials within the C–N–H system. Such compounds could also have applications for energy storage [4]. Analogous compounds include refractory ceramics based on Si_3N_4, Ga-, and Ge-containing nitrides that provide wide-bandgap materials for optoelectronics applications [5]. High-pressure, high-temperature (HPHT) synthesis experiments have resulted in spinel-structured forms of Si_3N_4 [6] and Ga_3O_3N [7, 8] with low compressibility, high hardness, and wide bandgaps. However, the synthesis of a purely crystalline form of carbon nitride phase under pressure has proved to be a challenging task, although some nonstoichiometric and amorphous C–N solids have been reported in previous experimental works [9].

Prepared from the molecular precursor dicyandiamide in the laser-heated diamond-anvil cell under HPHT conditions, Horvath-Bordon et al. [9] recently reported the synthesis of a well-crystallized compound with a N:C ratio of 3:2, carbon nitride imide $C_2N_2(NH)$ (see Fig. 1). This new dense carbon nitride phase can be recovered to a defect wurtzite structure (space group $Cmc2_1$, $Z = 4$) under ambient conditions. Their findings were confirmed by another following experiment study [10]. These experimental achievements have greatly stimulated the theoretical exploration of its novel physical properties to complement further experiments. Recently, the mechanical properties, electronic structure, and chemical

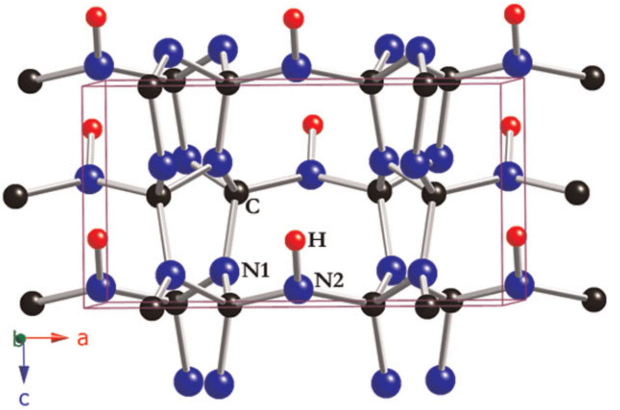

Figure 1 (online color at: www.pss-b.com) Crystal structure of $C_2N_2(NH)$; the large, middle, and small spheres represent N, C, and H atoms, respectively.

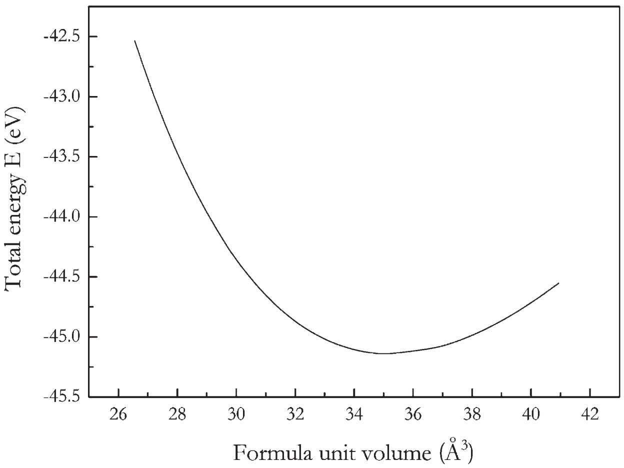

Figure 2 Total energy as a function of molecular volume for $C_2N_2(NH)$.

bonding of $C_2N_2(NH)$ have been investigated using the projector augmented-wave (PAW) method [11] based on density functional theory (DFT) [12] under ambient conditions [13]. This novel carbon nitride phase was found to be ultraincompressible and hard due to its high elastic moduli. In the present work, we extend the mechanical properties and present in detail the influence of elastic properties on the plastic deformation behavior and the role of the possible anisotropy of interatomic bonding. These will provide new insights into the excellent mechanical properties of $C_2N_2(NH)$. In addition, the structural and thermodynamic properties of the orthorhombic $C_2N_2(NH)$ under HPHT are also studied. The effects of pressure and temperature are systematically studied, and these can help us to further understand its potential applications under HPHT.

2 Computation details All structure relaxations were performed using DFT within the generalized gradient approximation (GGA) [14], as implemented in the Vienna *ab initio* simulation package [15]. The electron and core interactions were included by using the frozen-core all-electron PAW method [11], with H: $1s^1$, C: $2s^2 2p^2$, and N: $2s^2 2p^3$ treated as the valence electrons. The cutoff energy 520 eV for expansion of the wave function into plane waves was set for $C_2N_2(NH)$, and the special points sampling integration over the Brillouin zone was employed by using the Monkhorst–Pack method [16] with a grid of 0.03 Å^{-1} to obtain a well-converged total energy within 1 meV atom^{-1}. During the structural optimizations, all forces on atoms were converged to the order of 0.001 eV Å^{-1}, and the external stresses were reduced to be less than 0.01 GPa.

3 Result and discussions

3.1 Ground-state equilibrium properties The crystal structure of the $C_2N_2(NH)$ with $Cmc2_1$ space group is shown in Fig. 1. This compound contains two $C_2N_2(NH)$ formula units in a unit cell, in which four inequivalent atoms H, C, N1, and N2 occupy the Wyckoff 4*a* (0, 0.607, 0.203), 8*b* (0.671, 0.660, 0.998), 8*b* (0.699, 0, 0.416), and 4*a* (0, 0.719, 0.425) sites, respectively. The structural properties are the very important first step to understand the material properties from a microscopic point of view. The ground-state structure of $C_2N_2(NH)$ is investigated by the total energy electronic calculations over a wide range of the molecular volume V from 0.82 V_0 to 1.16 V_0, where V_0 is the zero-pressure equilibrium molecular volume. The calculated total energies as a function of the molecular volume for $C_2N_2(NH)$ are shown in Fig. 2. The equilibrium lattice constants, zero-pressure bulk modulus B_0, and its pressure derivative B_0' from the third-order Birch–Murnaghan equation of state (EOS) have been calculated in our previous work [13], which are the basis of our studies in this paper. In the present work, for the similar values at corresponding equilibrium lattice constants for GGA and LDA approaches, only the GGA results are presented in all calculations. Moreover, the pressure dependence of the normalized parameters a/a_0, b/b_0, and c/c_0 as a function of pressure for the $C_2N_2(NH)$ is exhibited in Fig. 3, where a_0, b_0, and c_0 is its value at $T = 0$ K and $P = 0$ GPa. By fitting the calculated data with least squares method, we obtained their relationships at the temperature of 0 K as the following relations:

$$\frac{a}{a_0} = 0.99991 - 1.31 \times 10^{-3} P + 5.73677 \times 10^{-6} P^2, \qquad (1)$$

$$\frac{b}{b_0} = 0.99961 - 1.47 \times 10^{-3} P + 6.54306 \times 10^{-6} P^2, \qquad (2)$$

$$\frac{c}{c_0} = 0.99977 - 0.933278 \times 10^{-3} P + 3.97542 \times 10^{-6} P^2. \qquad (3)$$

It can be clear seen that the compression along the *c*-axis is the smallest, consistent with the accumulation of CN_4

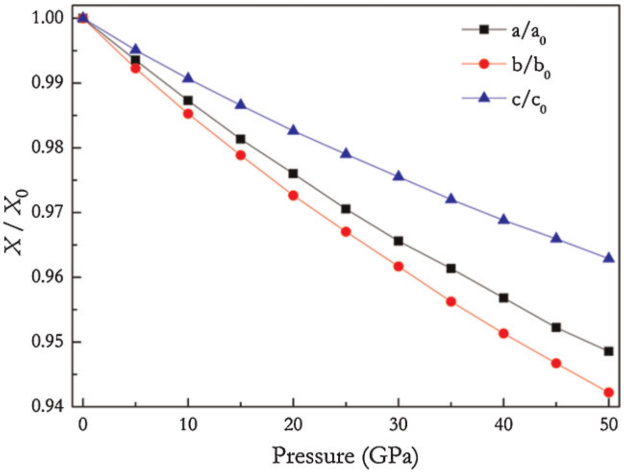

Figure 3 (online color at: www.pss-b.com) The normalized parameters $a/a_0, b/b_0, c/c_0$ as a function of the pressure for $C_2N_2(NH)$.

tetrahedron with strong C–N covalent bond along the *c*-axis. Moreover, this indicates clear elastic anisotropy of the $C_2N_2(NH)$.

3.2 Elastic anisotropy For the orthorhombic $C_2N_2(NH)$, the matrix of its elastic stiffness constants contains nine nonzero elements, *i.e.*, C_{11}, C_{12}, C_{13}, C_{22}, C_{23}, C_{33}, C_{44}, C_{55}, and C_{66}. The values of C_{ij} have been calculated in our previous work [13]. By using the relations between elastic compliance constants s_{ij} and the elastic constants C_{ij} [17, 18], the elastic compliance constants can be obtained. The values of C_{ij} and s_{ij} are collected in Table 1.

To calculate Young's modulus for a tensile stress applied along an arbitrary [*hkl*] direction, a variation of the Young's modulus along the arbitrary directions for orthorhombic symmetry can be written as [17]

$$E^{-1} = s_{11}\alpha^4 + s_{22}\beta^4 + s_{33}\gamma^4 + 2s_{12}\alpha^2\beta^2 + 2s_{23}\beta^2\gamma^2 \\ +2s_{13}\alpha^2\gamma^2 + s_{44}\beta^2\gamma^2 + +s_{55}\alpha^2\gamma^2 + s_{66}\alpha^2\beta^2, \tag{4}$$

where α, β, and γ are the direction cosines of the [*hkl*] direction. The directional dependence of the Young's modulus is shown in Fig. 4a, and the plane projections of the directional dependence of the Young's modulus in Fig. 4b for comparison. To study the anisotropy further, we can calculate the orientation dependence of Young's modulus when the tensile axis within specific planes. The formulas used in calculations are collected in Table 2 and the calculated results are plotted in Fig. 5a. Figure 5a shows that Young's modulus in $C_2N_2(NH)$ is the largest with $E_{\max} = 778$ GPa when the tensile axis is in the [001] direction, while on the contrary Young's modulus has its minimal value $E_{\min} = 526$ GPa along the [120] direction. This indicates that the $C_2N_2(NH)$ exhibits a pronounced anisotropy, namely $E_{\max}/E_{\min} = 1.48$. From the results in Fig. 5a, we can obtain the ordering of Young's modulus when the tensile axis along some specific direction as: $E_{[001]} > E_{[011]} > E_{[100]} > E_{[010]} \approx E_{[101]} \approx E_{[111]} > E_{[110]} > E_{[120]}$.

To understand plastic deformation in $C_2N_2(NH)$, the study of the dependence of the shear modulus on stress direction is useful. We choose a shear plane (*hkl*) and vary the shear stress direction [*uvw*] within that plane. The axis normal to the (*hkl*) plane is denoted as [*HKL*]. Thus, the shear modulus on the (*hkl*) shear plane with shear stress applied along [*uvw*] direction can be expressed as [17]

$$G^{-1} = 4s_{11}\alpha_1^2\alpha_2^2 + 4s_{22}\beta_1^2\beta_2^2 + 4s_{33}\gamma_1^2\gamma_2^2 \\ + 8s_{12}\alpha_1\alpha_2\beta_1\beta_2 + 8s_{23}\beta_1\beta_2\gamma_1\gamma_2 + 8s_{13}\alpha_1\alpha_2\gamma_1\gamma_2 \\ + s_{44}(\beta_1\gamma_2 + \beta_2\gamma_1)^2 + s_{55}(\alpha_1\gamma_2 + \alpha_2\gamma_1)^2 \\ + s_{66}(\alpha_1\beta_2 + \alpha_2\beta_1)^2, \tag{5}$$

where $\alpha_1, \beta_1, \gamma_1, \alpha_2, \beta_2, \text{and} \gamma_2$ are the direction cosines of the [*uvw*] and [*HKL*] directions. For shear plane (001) with the shear stress direction rotated from [100] to [010], the direction cosines are $\alpha_1 = \cos\theta$, $\beta_1 = \sin\theta$, $\gamma_1 = 0$, $\alpha_2 = \beta_2 = 0$, and $\gamma_2 = 1$, where θ is the angle between the [100] and shear stress direction. From Eq. (5), one can deduce the shear modulus on (001) as follows:

$$G^{-1}_{(001)} = s_{55} + (s_{44} - s_{55})\sin^2\theta. \tag{6}$$

For $C_2N_2(NH)$, $s_{44} < s_{55}$, the shear modulus is the largest along [010] and the smallest along [001].

When (100) is the shear plane, we rotate the shear stress direction from [001] to [010]. In Eq. (5), $\alpha_1 = 0$, $\beta_1 = \sin\theta$, $\gamma_1 = \cos\theta, \alpha_2 = 1, \beta_2 = \gamma_2 = 0$, then the shear modulus can be obtained as

$$G^{-1}_{(100)} = s_{55} + (s_{66} - s_{55})\sin^2\theta. \tag{7}$$

Since in our case, $s_{66} \approx s_{55}$, then $G^{-1}_{(100)} \approx s^{-1}_{55}$, which means that within the (100) plane, the shear modulus of $C_2N_2(NH)$ is nearly independent of the shear stress direction.

For the shear plane (010) with the shear stress direction rotated from [001] to [100],

$$G^{-1}_{(010)} = s_{44} + (s_{66} - s_{44})\sin^2\theta. \tag{8}$$

Table 1 The values of C_{ij} (in GPa) and s_{ij} (in 10^{-3} GPa^{-1}) for $C_2N_2(NH)$.

ij	11	22	33	12	23	13	44	55	66
C_{ij} [a]	597	567	804	89	79	107	335	221	222
s_{ij}	1.749	1.823	1.286	−0.245	−0.146	−0.209	2.985	4.524	4.505

[a] Ref. [13].

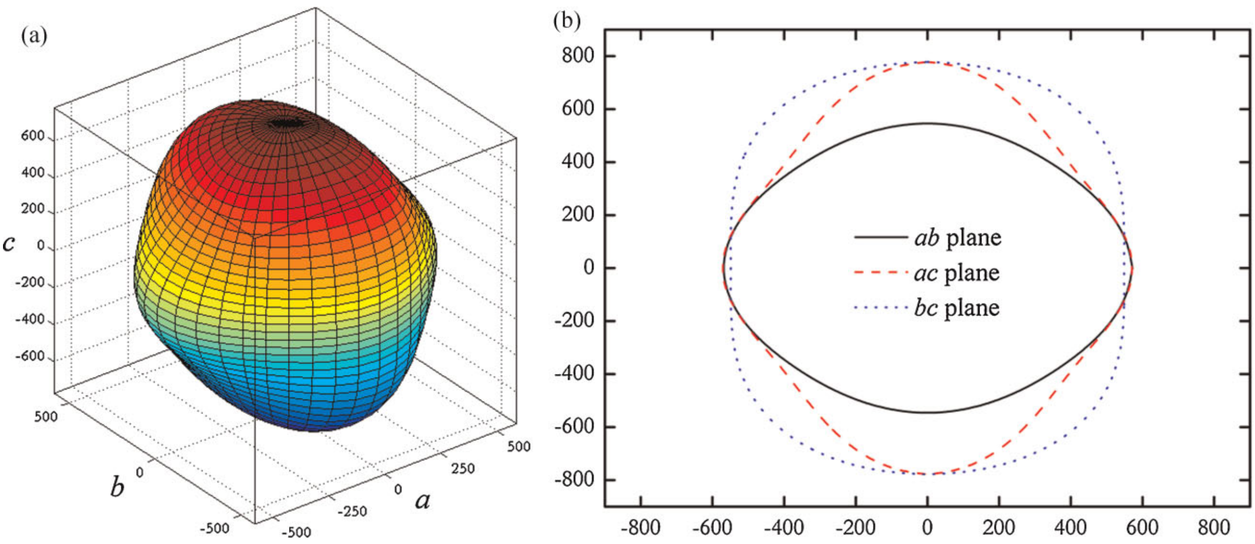

Figure 4 (online color at: www.pss-b.com) (a) Directional dependence of the Young's modulus in C_2N_2(NH). The plane projections of the directional dependence of the Young's modulus are shown in (b) for comparison.

Table 2 Formulas for the orientation dependence of Young's modulus when the tensile direction is rotated on specific planes.

tensile plane	E^{-1}	orientation angle
(001)	$s_{11}\cos^4\theta + s_{22}\sin^4\theta + 2s_{12}\sin^2\theta\cos^2\theta + s_{66}\sin^2\theta\cos^2\theta$	between [hk0] and [100]
(100)	$s_{22}\sin^4\theta + s_{33}\cos^4\theta + \frac{1}{4}(2s_{23} + s_{44})\sin^2 2\theta$	between [001] and [0kl]
(010)	$s_{11}\sin^4\theta + s_{33}\cos^4\theta + \frac{1}{4}(2s_{13} + s_{55})\sin^2 2\theta$	between [001] and [h0l]
$(1\bar{1}0)$	$\frac{\sin^4\theta}{(a^2+b^2)^2}[a^4 s_{11} + b^4 s_{12} + a^2b^2(2s_{12} + s_{66})] + s_{33}\cos^4\theta + \frac{\sin^2\theta\cos^2\theta}{a^2+b^2}[a^2(2s_{13} + s_{55}) + b^2(2s_{23} + s_{44})]$	between [001] and [hkl]

Due to $s_{44} < s_{66}$, the shear modulus is the largest along [001] with $G_{(010)[001]} = 335$ GPa and the smallest along [100] with $G_{(010)[100]} = 222$ GPa.

If the shear plane is $(1\bar{1}0)$, we rotate the shear stress from [001] to [110], then $\alpha_1 = \frac{a}{\sqrt{a^2+b^2}}\sin\theta$, $\beta_1 = \frac{b}{\sqrt{a^2+b^2}}\sin\theta$, $\gamma_1 = \cos\theta$, $\alpha_2 = \frac{b}{\sqrt{a^2+b^2}}$, $\beta_2 = -\frac{a}{\sqrt{a^2+b^2}}$, $\gamma_2 = 0$, where θ is the angle between [001] and the shear stress direction, a and b are the lattice constants. Then the shear modulus can be expressed as

$$G^{-1} = \frac{\sin^2\theta}{(a^2+b^2)^2}\left[a^2b^2(4s_{11} + 4s_{22} - 8s_{12}) + (b^2 - a^2)^2 s_{66}\right] + \frac{\cos^2\theta}{a^2+b^2}(a^2 s_{44} + b^2 s_{55}). \quad (9)$$

The orientation dependence of the shear modulus for the four cases discussed above is plotted in Fig. 5b. It can be seen from the figure that the shear modulus is the smallest on the (100) plane and almost independent of shear direction. This means that the (100) plane may be the cleavage plane of C_2N_2(NH).

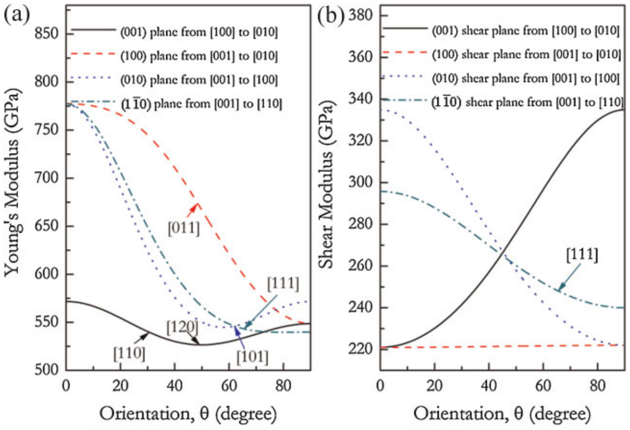

Figure 5 (online color at: www.pss-b.com) Orientation dependence of Young's modulus in C_2N_2(NH) (a) and orientation dependence of the shear modulus in C_2N_2(NH) (b).

3.3 Thermodynamic properties

The investigations on the thermodynamic properties of the orthorhombic C_2N_2(NH) under high temperature and pressure are determined by the quasiharmonic Debye model [19]. It should be noted that the Debye model of phonon density of states is essentially a linear extrapolation of the sound speed of acoustic branches but not optical branches in order to get density states. In fact, the thermodynamic properties of the crystal can be obtained by treating the lattice vibrations as quantized (phonons). Since this Debye model is very computationally quick and easy, it has been successfully applied to predict the thermodynamic properties of some materials [20–22]. The model has been described in detail in Ref. [19]. We only give a brief description as follows:

In the quasiharmonic Debye model, the nonequilibrium Gibbs function $G^*(V; P, T)$ is taken in the form of

$$G^*(V;P,T) = E(V) + PV + A_{\mathrm{Vib}}(\Theta(V);T), \tag{10}$$

where $E(V)$ is the total energy, PV corresponds to the constant hydrostatic pressure condition, $\Theta(V)$ is the Debye temperature, and the vibrational contribution A_{Vib} can be written as

$$A_{\mathrm{Vib}}(\Theta(V),T) = nkT\left[\frac{9}{8}\frac{\Theta}{T} + 3\ln(1-e^{-\Theta/T}) - D\left(\frac{\Theta}{T}\right)\right]. \tag{11}$$

Here n is the number of atoms per formula unit, and the Debye integral $D(\Theta/T)$ is defined as [19]

$$D(y) = \frac{3}{y^3}\int_0^y \frac{x^3}{\mathrm{e}^x - 1}\mathrm{d}x. \tag{12}$$

For an isotropic solid, Θ is expressed as

$$\Theta = \hbar(6\pi^2 V^{1/2} n)^{1/3} f(\sigma)\sqrt{\frac{B_{\mathrm{S}}}{k_{\mathrm{B}}{}^2 M}}, \tag{13}$$

where V, M, and n is the molecular volume, molar mass, the number of atom per formula unit. A scaling function, $f(\sigma)$, which depend on Poisson's ratio of the isotropic solid is given by [23, 24]

$$f(\sigma) = \left\{3\left[2\left(\frac{2}{3}\cdot\frac{1+\sigma}{1-2\sigma}\right)^{3/2} + \left(\frac{1}{3}\cdot\frac{1+\sigma}{1-\sigma}\right)^{3/2}\right]^{-1}\right\}^{1/3}. \tag{14}$$

Here, the Poisson ratio σ is taken as 0.137 [13], $f(\sigma) = 0.748661$. The B_S is the adiabatic bulk modulus, which can be approximated by the static compressibility

$$B_S \cong B(V) = V\left(\frac{\mathrm{d}^2E(V)}{\mathrm{d}V^2}\right). \tag{15}$$

Therefore, the nonequilibrium Gibbs function G^* as a function of (V; P, T) can be minimized with respect to volume V as

$$\left(\frac{\partial G^*(V;P,T)}{\partial V}\right)_{P,T} = 0. \tag{16}$$

By solving Eq. (16), one can get the thermal EOS $V(P, T)$. The isothermal bulk modulus and other thermal properties such as heat capacity C_V and C_P, the relationship of B_S and B_T, and the thermal expansion α are, respectively, taken as:

$$B_T(P,T) = -V\left(\frac{\partial P}{\partial V}\right) = \left(\frac{\partial^2 G^*(V;P,T)}{\partial V^2}\right)_{P,T}, \tag{17}$$

$$C_V = 3nk\left[4D(\Theta/T) - \frac{3\Theta/T}{e^{\Theta/T}-1}\right], \tag{18}$$

$$C_P = C_V(1+\alpha\gamma T), \tag{19}$$

$$B_S = B_T(1+\alpha\gamma T), \tag{20}$$

$$\alpha = \frac{\gamma C_V}{B_T V}, \tag{21}$$

where γ is the Grüneisen parameter defined as

$$\gamma = -\frac{\mathrm{d}\ln\Theta(V)}{\mathrm{d}\ln V}. \tag{22}$$

The Debye model with quasiharmonic approximation has its shortcomings [25]: (i) the anharmonic interatomic interaction is more pronounced at higher temperature; (ii) the Debye model is developed for crystalline solids, thus when the temperature approaches the melting point, the system is no longer an ideal crystalline solid and the model will become less reliable. In the present work, the thermal properties of the $C_2N_2(NH)$ are determined in the temperature range from 0 to 2000 K, which is within the actual experimental conditions. Therefore, the quasiharmonic model used here is reliable and reasonable.

In the quasiharmonic Debye model, the Debye temperature Θ and the Grüneisen parameter γ are two key quantities. The Debye temperature closely relates to many physical properties of solids, such as specific heat, dynamic properties, and melting temperature [26]. The Grüneisen parameter describes the anharmonic effects in the vibrating lattice, and it has been widely used to characterize and extrapolate the thermodynamic behavior of a material at HPHT. The Debye temperature and the Grüneisen parameter at various temperatures (0, 300, 600, 1200, and 2000 K) and different pressures (0, 10, 20, 30, 40, 50, and 60 GPa) are listed in Table 3. In this work, we obtained the Debye temperature $\Theta = 1525.7$ K at $P = 0$ GPa and $T = 0$ K. this is smaller than the result (1658 K) calculated by elastic constants in our previous work [13]. It can be seen from Table 3 that, when the applied pressure is from 0 to 60 GPa, the Debye temperature increases by 23.9, 24.1, 24.7, 26.5, and 29.7% at temperatures of 0, 300, 600, 1200, and 2000 K, respectively. This indicates that the Debye temperature Θ increases more

Table 3 Calculated Debye temperature Θ (in K) and Grüneisen parameter γ of orthorhombic $C_2N_2(NH)$ at different pressures and different temperatures.

T (K)	P (GPa)							
	parameter	0	10	20	30	40	50	60
0	Θ	1525.7	1621.4	1709.2	1790.4	1866.3	1937.7	2005.4
	γ	1.623	1.577	1.542	1.516	1.496	1.481	1.469
300	Θ	1521.7	1618.3	1706.7	1788.3	1864.4	1936.1	2004.0
	γ	1.625	1.578	1.543	1.517	1.497	1.481	1.469
600	Θ	1500.9	1600.9	1691.4	1774.7	1852.1	1924.9	1993.7
	γ	1.637	1.586	1.549	1.521	1.500	1.484	1.471
1200	Θ	1437.0	1544.9	1641.0	1728.5	1809.2	1884.6	1955.6
	γ	1.676	1.613	1.568	1.536	1.511	1.492	1.478
2000	Θ	1330.8	1453.9	1559.7	1654.1	1740.1	1819.6	1893.8
	γ	1.757	1.665	1.605	1.563	1.532	1.508	1.490

quickly at high temperature than at low temperature. When carefully examined, one can find that Θ increases almost linearly with applied pressures. As the Grüneisen parameter γ has anharmonic behavior, we would not expect linear variation with pressure P and temperature T. At given pressure, the γ increases dramatically with the temperature T when $T > 600$ K and varies almost monotonously with temperature T. While at fixed temperature, the γ decreases dramatically with increasing pressure, and the decrease becomes more rapid with the increasing temperature. These results show that the effect of temperature T on the ratio γ is not as significant as that of pressure P, and there will be a large thermal expansion at a low pressure P.

The variations of the heat capacity at constant pressure C_P and the constant volume heat capacity C_V with temperature T and pressure P are also investigated, as shown in Fig. 6. The difference between C_P and C_V is very small at low temperatures. At high temperatures, the C_V approaches a constant value, C_P increases monotonously with increments of the temperature. On the other hand, the difference between the C_P and the C_V decreases with increasing pressure. It is also interesting to note that the values of C_V follow the Debye model at low temperature due to the anharmonic approximations. The anharmonic effect on C_V is suppressed and the C_V is close to a constant at sufficiently high temperatures, obeying Dulong and Petit's Rule. In summary, one can see that the heat capacity increases with the temperature at the same pressure and decreases with the pressure at the same temperature. The influences of the temperature on the heat capacity are much more significant than that of the pressure on it.

In Fig. 7, we present the change in thermal expansion coefficient α with pressure and temperature for $C_2N_2(NH)$. At $T = 300$ K and $P = 0$ GPa, the calculated α is $1.64 \times 10^{-5}\,K^{-1}$ in the present work. In Fig. 7a, it is noted that as the pressure increases, α almost decreases exponentially. This means that there is a large thermal expansion at low pressure, which is in accordance with the variation of V with pressure P. Moreover, the effects of the pressure P on

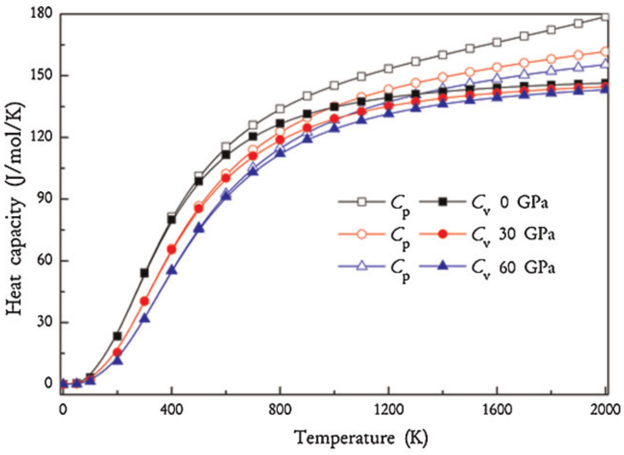

Figure 6 (online color at: www.pss-b.com) Temperature dependence of the heat capacity at different pressures for $C_2N_2(NH)$.

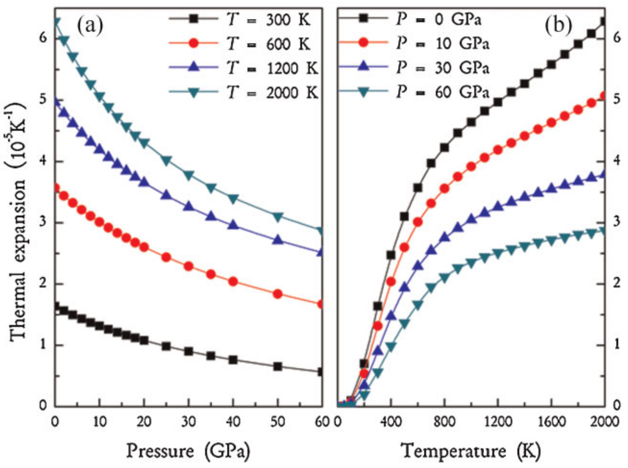

Figure 7 (online color at: www.pss-b.com) Pressure (a) and temperature (b) dependence of the thermal expansion coefficient α for $C_2N_2(NH)$.

the thermal expansion coefficient α are very small at low temperature, and as the temperature T increases, the effects become obvious. That is to say, the higher the temperature T is, the faster the α decreases, as shown in Fig. 7a. From Fig. 7b, the thermal expansion coefficient α increases with T^3 at low temperatures and gradually approaches a linear increase at high temperatures. Finally, the increasing trend becomes gentler. It should be noted that the thermal expansion coefficient α converges to a constant value at high temperatures and pressures. Moreover, the impact of temperature is much greater than the impact of pressure on the thermal expansion coefficient α, which is similar to C_V. These results are in accordance with the results of the Debye theory that applies to many materials.

The experimental data about the Debye temperature, Grüneisen parameter, heat capacity, and expansion coefficient of $C_2N_2(NH)$ under HPHT are not yet available for comparison, but considering the case of Refs. [27, 28], our predicted values should be credible. We hope that future experimental measurements will verify all these calculated results.

4 Conclusions The structural, elastic anisotropy, and thermodynamic properties of $C_2N_2(NH)$ are successfully investigated using the plane-wave pseudopotential density theory method in combination with the quasiharmonic Debye model. The Young's modulus in $C_2N_2(NH)$ varies with the tensile direction. For the principal crystal directions, the calculations show the order $E_{[001]} > E_{[011]} > E_{[100]} > E_{[010]} \approx E_{[101]} \approx E_{[111]} > E_{[110]} > E_{[120]}$. This means that the crystal is stiffer when deformed uniaxially along the [001] direction. This is attributed to the accumulation of CN_4 tetrahedron with strong C–N covalent bonds along the c-axis. The shear modulus of $C_2N_2(NH)$ is the largest on the (001) with the [010] shear stress direction and on (010) with the [001] shear stress direction. The smallest shear modulus on the (100) plane means that the (100) plane may be the cleavage plane of $C_2N_2(NH)$. Using the quasiharmonic Debye model, the thermodynamic properties including the Debye temperature, Grüneisen parameter, the heat capacity, and the thermal expansion coefficients are predicted under HPHT. The result shows that the Debye temperature Θ increases linearly with pressure and decreases with increasing temperature, especially at high temperatures. High pressure gives rise to a smaller Grüneisen parameter, heat capacity, and thermal expansion coefficients at constant temperature. However, high temperature leads to a larger Grüneisen parameter, a larger heat capacity, and a larger thermal expansion coefficient at constant pressure.

Acknowledgements This work is supported by the National Natural Science Foundation of China under (Grant No. 11204007), the Natural Science Basic Research plan in Shaanxi Province of China (Grant No. 2012JQ1005), the Fundamental Research Funds for the Central Universities, and the Baoji University of Arts and Sciences Key Research (Grant No. ZK11060).

References

[1] R. B. Kaner, J. J. Gilman, and S. H. Tolbert, Science **308**, 1268–1269 (2005).
[2] A. Y. Liu and M. L. Cohen, Science **245**, 841–842 (1989).
[3] D. M. Teter and R. J. Hemley, Science **271**, 53–55 (1996).
[4] X. C. Wang, K. Maeda, A. Thomas, K. Takanabe, G. Xin, J. M. Carlsson, K. Domen, and M. Antonietti, Nature Mater. **8**, 76–80 (2009).
[5] F. A. Ponce and D. P. Bour, Nature **386**, 351 (1997).
[6] E. Soignard, M. Somayazulu, J. Dong, O. F. Sankey, and P. F. McMillan, J. Phys.: Condens. Matter **13**, 557–564 (2001).
[7] I. Kinski, G. Miehe, G. Heymann, R. Theissmann, R. Riedel, and H. Huppertz, Z. Naturforsch. B **60**, 831–836 (2005).
[8] E. Soignard, D. Machon, P. F. McMillan, J. Dong, B. Xu, and K. Leinenweber, Mater. Chem. **17**, 5465–5472 (2005).
[9] E. Horvath-Bordon, R. Riedel, P. F. McMillan, P. Kroll, G. M. A. v. Aken, A. Zerr, P. Hoppe, O. Shebanova, L. McLaren, S. Lauterbach, E. Kroke, and R. Boehler, Angew. Chem., Int. Ed. **46**, 1476–1480 (2007).
[10] A. Salamat, K. Woodhead, P. F. McMillan, R. Q. Cabrera, A. Rahman, D. Adriaens, F. Cora, and J. P. Perrillat, Phys. Rev. B **80**, 104106 (2009).
[11] P. E. Blöchl, Phys. Rev. B **50**, 17953–17979 (1994).
[12] P. Hohenberg and W. Kohn, Phys. Rev. **136**, B864–B871 (1964).
[13] H. Y. Yan, Q. Wei, B. B. Zheng, and P. Guo, J. Solid State Chem. **184**, 572–577 (2011).
[14] D. M. Ceperley and B. J. Alder, Phys. Rev. Lett. **45**, 566–569 (1980).
[15] G. Kresse and D. Joubert, Phys. Rev. B **59**, 1758–1775 (1999).
[16] H. J. Monkhorst and J. D. Pack, Phys. Rev. B **13**, 5188–5192 (1976).
[17] Y. He, R. B. Schwarz, A. Migliori, and S. H. Whang, J. Mater. Res. **10**, 1187–1195 (1995).
[18] Q. J. Liu, Z. T. Liu, L. P. Feng, and H. Tian, Solid State Sci. **13**, 1076–1082 (2011).
[19] M. A. Blanco, E. Francisco, and V. Luaña, Comput. Phys. Commun. **158**, 57–72 (2004).
[20] Y. O. Ciftci, M. Ozayman, G. Surucu, K. Colakoglu, and E. Deligoz, Solid State Sci. **14**, 401–408 (2012).
[21] B. Ghebouli, M. A. Ghebouli, M. Fatmi, and A. Bouhemadou, Solid State Commun. **150**, 1896–1901 (2010).
[22] X. F. Li, Z. L. Liu, C. L. Ding, H. Z. Fu, and G. F. Ji, Mater. Chem. Phys. **130**, 14–19 (2011).
[23] E. Francisco, J. M. Recio, M. A. Blanco, A. Marín Pendás, and A. Costales, J. Phys. Chem. A **102**, 1595–1601 (1998).
[24] E. Francisco, M. A. Blanco, and G. Sanjurjo, Phys. Rev. B **63**, 094107 (2001).
[25] F. Peng, Q. Liu, H. Fu, and X. Yang, Solid State Commun. **149**, 56–59 (2009).
[26] P. Ravindran, L. Fast, P. A. Korzhavyi, B. Johansson, J. Wills, and O. Eriksson, J. Appl. Phys. **84**, 4891–4904 (1998).
[27] T. Litaka and T. Ebisuzaki, Phys. Rev. B **65**, 012103 (2001).
[28] O. Gülseren and R. E. Cohen, Phys. Rev. B **65**, 064103 (2002).